International Journal on Heart and Vascular system

An Atrial Fibrillation-Associated Variant of Nup155 Maintains Stable Dynamics at the Nuclear Envelope

Research Article

Volume 2 Issue 2- 2022

Author Details

*Storm EC[1], Preston C[1, 2] and Faustino R[1, 3]**

[1]*Genetics and Genomics Group, Sanford Research, USA*

[2]*Biology Department, St. Mary's University of Minnesota, USA*

[3]*Department of Paediatrics, Sanford School of Medicine (SSOM) of the University of South Dakota, USA*

*Corresponding author

Randy Faustino, Department of Paediatrics, Sanford School of Medicine of the University of South Dakota, 1400 W. 22nd Street, Sioux Falls, SD 57105, USA

Article History

Received: November 05, 2022 Accepted: November 09, 2022 Published: November 09, 2022

Abstract

Background: Nuclear pore complex proteins are associated with developmental diseases, but the mechanism of action remains poorly characterized. This study focused on a clinically reported, atrial fibrillation-associated variant of nucleoporin NUP155 to gain insight into potential mechanisms underlying its associated phenotype.

Methods: Fluorescent mobility assays were used to assess subcellular localization and dynamics of stably expressed, GFP-tagged exogenous NUP155-R391H and compare its mobility and residency time at the nuclear envelope.

Results: NUP155 exhibits a mean nuclear envelope residence time of 15.6 hrs comparable to other stable members of the nuclear pore complex. NUP155 demonstrates monophasic decay kinetics that correspond to one slow-exchanging pool, and the clinical NUP155-R391H variant showed comparable stability and decay kinetics to wild type NUP155, with a mean residence time of 15.4 hrs.

Conclusion: NUP155-R391H is comparable to wild type NUP155 localization and nuclear envelope residency dynamics, implicating alternative NUP155 functions driving reported clinical cardiac phenotypes.

Keywords: Nuclear pore complex; Nucleoporin; Inner ring complex; Fluorescence assay; iFRAP; Decay kinetics

Abbreviations: IFRAP: Inverse Fluorescent Recovery After Photo bleaching; NUP: Nucleoporin; NPC: Nuclear Pore Complex

Introduction

The nuclear pore complex (NPC) is a large protein complex that allows for nucleocytoplasmic communication and maintains a stable position due to its association with the nuclear lamina [1]. Despite this stability, individual components of the NPC, termed nucleoporins (nups) have variable half-lives and mobilities [2,3] which can vary by several orders of magnitude, from seconds to days [4]. These unique and sometimes tissue specific dynamics [5] may factor into the role of nups in development and disease [6-8]. Among these, NUP155 has emerged as having an essential role in cardiac physiology and has been clinically associated with atrial fibrillation and sudden cardiac death [9,10]. Specifically, the NUP155 R391H point mutation was linked to familial neonatal atrial fibrillation and sudden cardiac death, with initial supporting studies implicating specific transport defects in HSP70 that precipitated cardiomyocyte compromise [9].

Building on this, subsequent work identified a potential role for NUP155 in regulating chromatin access and conformation [11], supported by recent studies that revealed global transcriptome changes in NUP155-R391H stem cell lines [12, 13]. In parallel with these emerging genome/transcriptome regulatory functions, the operational diversity of the NPC may also include sophisticated control of protein turnover. In yeast, reports of Trp homologues Mlp1p and Mlp2p [14] interacting with proteasomal components [15] suggested that the NPC contributes to functions beyond the NPC proper. This was further corroborated by independent work that identified proteasome subunits at two NPC sites [16], implicating proteasomal localization at the NPC may be critical for regulating local protein turnover, such

as those involved in kinetochore function and proper chromosome dynamics [17]. NUP155 is a stable essential component of the NPC which when disrupted redistributes to the cytoplasm [18-21], underscoring the importance of NUP155 in proper NPC maintenance.

However, the specific mechanism(s) by which NUP155 and its R391H mutation contribute to cardiac pathology remains elusive. This study examines localization dynamics of NUP155 and the impact of the R391H mutation in the setting of cellular stress. Understanding these functions of NUP155 and the specific impact of the R391H mutation will provide a better understanding of NUP155 biology to facilitate identification of cellular mechanisms that may ultimately underlie the associated clinical pathology.

Materials and Methods

Plasmid Design

3GFP-tagged nup fusion proteins were designed using a pBABE vector to test the mobility of NUP155, the clinically identified mutant NUP155-R391H, and three previously established controls: NUP35, NUP85, and NUP153. The NUP155-R391H variant was generated by polymerase chain reaction (PCR) mutagenesis, where primers containing the point mutation were used to introduce the R391H mutation while amplifying distal and proximal segments of the Coding Sequence region (CDS). All the primer sequences and PCR cycle details used in this study are found in (Table 1).

Table 1

CloneAmp HiFi PCR Cycle:	1. 98°C for 30 sec	
	2. 98°C for 10 sec	
	3. (Variable*)°C for 20 sec annealing (*based on the lower annealing temperature of primer pair)	
	4. 72°C for (Variable*) sec extension (*15 sec/kb, based on the size of amplicon)	
	5. Repeat steps 2-4 29x	
	6. 72°C for 10 min	
	7. 4°C indefinitely	
Primer Sequence (5' - 3')	**Annealing Temp °C**	**Description**
TACAAGTACTCAGATCTCGAGATGCCATCGGTGCTG	71.47	Amplify 3GFP
ATCAGCGGTTTAAACCTTAAGATGGAGCCGTTCCAG	69.85	Amplify 3GFP
TGTGGTGGTACGTAGGAATTCTGGCTAGCCACCATG	69.51	Amplify Nup155
CACACATTCCACAGGGTCGACTTAAACCTTAAGATGGAG	69.13	Amplify Nup155
ACACTGGTCCACGTCCACTTACCTCCTGGATTT	67.6	Generate R391H
AAATCCAGGAGGTAAGTGGACGTGGACCAGTGT	67.6	Generate R391H
GTACTCAGATCTCGAGATGGCCTCGGAAGCCG	71.6	Amplify Nup153
ATTCCACAGGGTCGACTTATTTCTTGCGTCTAACAGCAGTCTTTATCTTG	73.74	Amplify Nup153
GTACTCAGATCTCGAGATGGAGGAGCTCGACTGCG	73.3	Amplify Nup85
ATTCCACAGGGTCGACTCAGGAACCCTCCAGTGAGC	71.92	Amplify Nup85
AGTACTCAGATCTCGAGATGGCAGCGTTTGCGG	72.37	Amplify Nup35
ACACATTCCACAGGGTCGATTACCAACCGAACATGTACTCCATCG	72.48	Amplify Nup35

Cell Culture and Stable Line Generation

Immortalized mouse fibroblasts NIH/3T3 (ATCC®, CRL-1658™, Manassas, VA) stably expressing the fluorescent constructs were generated using retroviral transduction. Viral production was achieved using Phoenix-AMPHO cells (ATCC®, CRL-3213™, and Manassas, VA).

Fluorescent Mobility Assays

The imaging method utilized for assessing mobility of our fluorescent protein fusions is inverse fluorescence recovery after photo bleaching (iFRAP) [22]. Briefly, NIH/3T3 fibroblasts stably expressing 3GFP-tagged nups were plated on FluoroDishes (35mm) prior to performing iFRAP experiments. Imaging fields (40x) were selected

to ensure at least three cells, with clear nuclear envelope localization of the 3GFP-tagged constructs, were visible at the same z-plane for comparable control and reference measurements.

Data Processing and Analysis

Following acquisition of fluorescent data, measurements and analysis of the regions of interest (ROI) were performed using the NIS-Elements AR imaging software (v5.20.02; Nikon Corporation, Tokyo, Japan). ROIs for background, bleached and unbleached areas, and reference areas for each selected cell were determined prior to analysis according to previously reported methods [4]. Tracking features within the software were used to account for cell movement during the experiment. Background fluorescence intensity was subtracted from all bleached and unbleached measurements at their respective time points. These corrected values were then normalized to the first post-bleach measurement. The dissociation kinetics of each 3GFP-tagged nup was calculated using the following formula [4]:

$$D(t - t_{post}) = \frac{\frac{I_U(t) - I_R(t)}{I_U(t_{pre}) - I_R(t_{pre})} - \frac{I_B(t) - I_R(t)}{I_B(t_{pre}) - I_R(t_{pre})}}{\frac{I_U(t_{post}) - I_R(t_{post})}{I_U(t_{pre}) - I_R(t_{pre})} - \frac{I_B(t_{post}) - I_R(t_{post})}{I_B(t_{pre}) - I_R(t_{pre})}}$$

I_U refers to the fluorescence intensity of the unbleached ROI; I_B refers to fluorescence intensity measurement of the bleached ROI and I_R refers to the background fluorescence intensity ROI. t_{pre} refers to the average pre-bleach measurement and t_{post} is the post-bleach value. The dissociation kinetics (D(t)) was determined subtracting the fluorescence of the bleached (t_{post}) from the unbleached at each measured time point for each nup. The calculated values were exported into GraphPad Prism 8 software (GraphPad Software, San Diego, CA) for analysis and visualization of data. Values for each 3GFP-tagged nup was analyzed using an exponential decay equation (fitted to one or two-phase decay). The dissociation rate (K_{off}) was used to calculate the residency time of each nup, calculated as $1/K_{off}$.

Results

NUP153, NUP35 and NUP85 are previously characterized nups selected as iFRAP controls for comparative evaluation of NUP155 mobility at the nuclear envelope [4]. These nups were chosen as benchmarks for their varied sub complex distribution within the NPC as well as their residence times within the nuclear envelope [4]. Our results demonstrated that 3GFP-NUP153 and 3GFP-NUP35 exhibit dissociation rates in line with previous reports (Figure 1A, 1D). The dissociation rate calculated for 3GFP-NUP85 in our study was higher than previously reported. In addition, NUP85 exhibited a long-lasting residency time of ~20 hrs (Figure 1E, 1F). NUP155 is a component of the inner ring complexed with NUP35, NUP93, NUP188 and NUP205 [23]. While NUP155 protein half-life exhibits low turnover [23, 24], its mobility and residency at the nuclear envelope is unknown. For the present iFRAP study, a 3GFP-NUP155 construct was used to investigate the dissociation kinetics and residence time of NUP155 (Figure 2A, 2B).

Our findings revealed that 3GFP-NUP155 exhibited a calculated koff of 1.78 ± 0.14 x 10^{-5} per second (Figure 2C). In parallel, we examined the mobility of a NUP155 variant associated with atrial fibrillation, i.e. an R-H missense mutation at amino acid 391 [9], to determine if that mutation possessed different kinetics than wild type. Results of the 3GFP-NUP155-R391H reporter were comparable to the 3GFP-NUP155 data, with a calculated koff of 1.80 ± 0.20 x 10^{-5} per second (Figure 2D). Furthermore, when considered alongside NUP85, NUP155 and NUP155-R391H revealed comparable exponential decay curves with no statistical difference in dissociation rates among the three (p-value = 0.1663) (Figure 3A). Significantly, 3GFP-NUP155 exhibited a residence time at the nuclear envelope of 15.6 hours, with a comparable residency time of 15.4 hours determined for 3GFP-NUP155-R391H (Figure 3B).

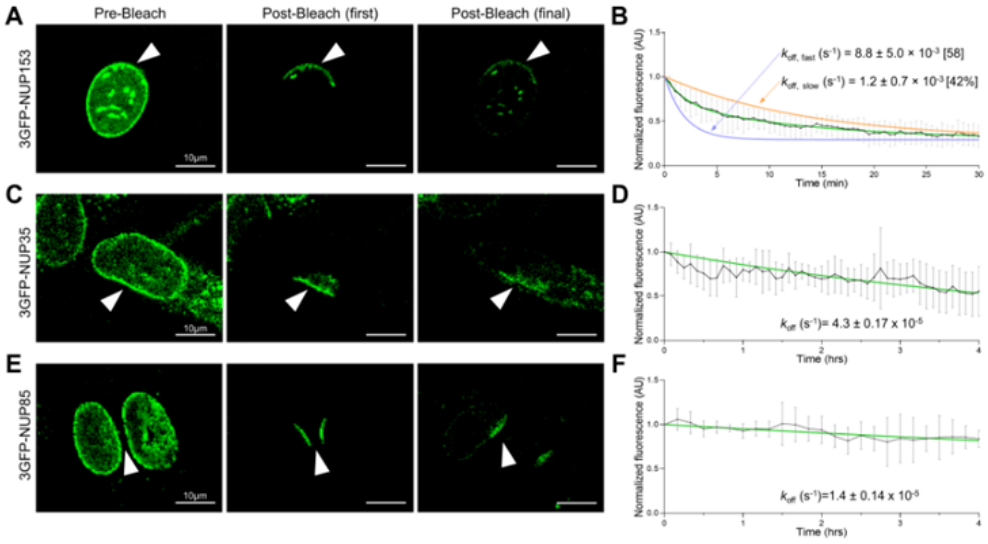

Figure 1: Different nucleoporins display a range of dissociation kinetics. A. Representative time-lapse images of NIH3T3 fibroblasts express-ing fluorescent GFP-tagged NUP153 showing a pre-bleach image (first row panel), the first post-bleach image (second row panel), and the fi-nal post-bleach image (third row panel) during a single iFRAP experiment. White arrowheads indicate the unbleached region of interest (ROI) monitored during the experiment. B. Dissociation kinetics for NUP153 (n = 6) depicting a biphasic decay dissociation curve (green) as a result of two dissociation rates for NUP153: K_{off}, fast curve shown in light blue and K_{off}, slow shown in orange. C. Representative images and D. dis-sociation kinetics for NUP35 (n = 11) showing a monophasic dissociation curve (green) during 4 hr iFRAP experiments. E. Representative im-ages and F. dissociation kinetics for NUP85 (n = 11). Scale bars represent 10 μm.

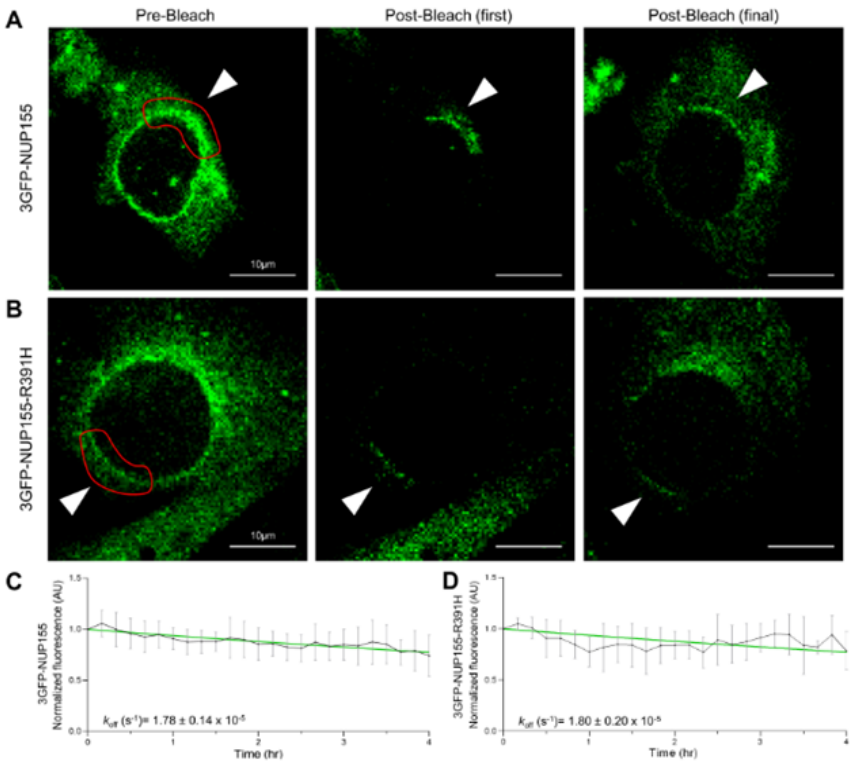

Figure 2: The clinical NUP155-R391H variant exhibits a stable dissociation rate comparable to wild type NUP155. A & B. Representative time-lapse panels of NIH3T3 fibroblasts expressing fluorescent wild type NUP155 and the NUP155-R391H variant showing pre-bleach, first post-bleach and final post-bleach images during iFRAP experiments. White arrowheads indicate un-bleached ROI tracked throughout the course of the experiments. Scale bar represents 10 μm. C & D. Dissociation kinetics of fluorescently tagged wild type NUP155 and NUP155-R391H (n = 10 for each group) showing monophasic dissociation curves (green) with comparable dissociation rates (NUP155, K_{off} = 1.78 ± 0.14 x 10^{-5}; NUP155-R391H, K_{off} = 1.80 ± 0.20 x 10^{-5}) during 4 hr iFRAP experiments.

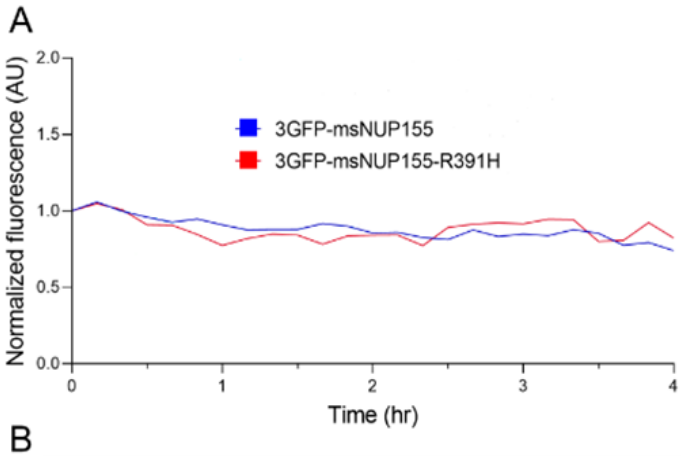

B

Protein ID	k_{off} (s^{-1})	Residence time ($1/k_{off}$)
NUP153	slow 1.2 ± 0.7 × 10^{-3} [42%]	14 min.
	fast 8.8 ± 5.0 × 10^{-3} [58%]	114 sec.
NUP35	4.34 ± 0.17 x 10^{-5}	6.5 hr.
NUP85	1.40 ± 0.14 x 10^{-5}	19.8 hr.
NUP155	1.78 ± 0.14 x 10^{-5}	15.6 hr.
NUP155-R391H	1.80 ± 0.20 x 10^{-5}	15.4 hr.

Figure 3: NUP155 and its clinical variant, NUP155-R391H, exhibit stable dynamics at the nuclear envelope. A. This graph depicts curve similarities in dissociation kinetics among wild type NUP155 (blue) and NUP155-R391H (red), establishing their stability as long-lived proteins. B. Table providing dissociation rates (K_{off}, average rates from at least 6 experiments) and residence times for NUP153, NUP35, NUP85, NUP155 and NUP155-R391H. Long-lived residency times of 15.6 hrs and 15.4 hrs were respectively identified for NUP155 and NUP155-R391H in the current study.

Discussion

In the present study, we show for the first time that the NUP155 R391H variant does not significantly change protein mobility and/or residence time at the nuclear envelope. Earlier work using a LacI/LacO reporter system provided evidence that NPC sub complex formation and nuclear envelope localization was impaired in NUP155-R391H mutants expressed in an immortalized aneuploidy osteosarcoma cell line [25]. This phenotype of deficient nup recruitment was ascribed to the impaired interactions between NUP155 and its binding partners NUP35 and membrane-bound POM121 [25]. However, subsequent work by an independent group reported proper nuclear pore complex assembly and NE localization of the NUP155-R391H variant [26]. These latter findings are in line with our current results showing that NUP155 and NUP155-R391H stably localize to the nuclear envelope. Indeed, it has been suggested that the homozygous NUP155-R391H expression causes a much milder NPC dysfunction, and that any pathological effects of the NUP155 mutation may be related to a discrete functional deficit distinct from the NPC assembly properties of NUP155 [26].

For example, it has been demonstrated that proteins of the inner nuclear membrane are recruited by other regions of NUP155 distinct from its N-terminal beta-propeller domain in which R391 is found [27, 28]. Indeed, the alpha-solenoid C-terminal domain of NUP155 interacts with other proteins [11, 29]. Moreover, given the endogenous auto inhibitory self-interaction between the N-and C- terminus of NUP155 [26], any disruptions to this innate interaction could increase temporal exposure of binding surfaces on either domain, leading to alterations in the NUP155 interact me with attendant downstream functional effects.

The controls used in present study exhibited similar stabilities as reported previously [4]. Functionally, the residency times for each of the representative nups selected for the present study are in line with their function within the NPC. For example, NUP153 is a highly mobile member of the nuclear basket that dynamically interacts with chromatin to regulate gene expression [4, 19-21, 30].

NUP85 is a stable component of the Y-sub complex with a long residency time that forms one of the arms of the "Y" and helps create a hydrophobic core within the sub complex essential for its role as the main scaffolding component of the NPC [4,31]. NUP35 plays a critical role in NPC biogenesis [32,33], and is part of the inner ring complex that mediates interactions between the central channel and the Y-sub complexes of the NPC outer ring [23,34]. In addition, NUP35 functions as an RNA-binding post-transcriptional regulator [35,36]. With respect to the residency time of NUP35, it is intermediate between that of NUP153 and NUP85 [4].

Conclusions

Our experiments show NUP155 is stably localized to the nuclear envelope, with long residency times that reflect its biochemical stability [24]. Furthermore, our findings indicate that the R391H mutation in NUP155 does not impair this stability. This implicates the role of other potential molecular functions for NUP155 that may underlie the clinically observed NUP155-R391H associated cardiopathology.

Future Directions

A potential functional area that may be impacted is the protein interactome associated with NUP155. To address this, future studies investigating the NUP155 interactome in both wild type as well as mutant conditions, will provide more information to understand protein-protein network functions of NUP155 that may be impacted by the R391H mutation. In addition, while the localization of NUP155 to the nuclear envelope is confirmed by our present work, the potential distribution of NUP155 to non-NPC complexes within the nuclear envelope [37] cannot be resolved. To address this, super-resolution microscopy as well as correlative light electron microscopy would provide increased levels of granularity to identify potential NPC-localized versus NPC-independent pools of NUP155.

Limitations

Data from the present study were acquired in immortalized murine fibroblasts, which may not identify changes that occur in a cardiac cell where the NUP155-R391H mutation and phenotype were first observed. Given the tissue specific expression patterns of NUP155 [38], it is possible that the pathogenic effects of the homozygous NUP155-R391H mutation are observed in cell/tissue types where effects of the mutation would be compounded by high endogenous NUP155 expression. Performing these experiments in a cardiac cell type would provide context-specific information on the effects of NUP155 impairment. Indeed, comparative assessment of NUP155 effects in multiple cell types will provide a broader comprehensive measure of NUP155 function in different tissue types, as the current study limits our observations to a non-normal immortalized cell line.

Acknowledgements

We would like to gratefully acknowledge all the assistance with imaging techniques kindly provided by Kelly Graber and Indra Chandrasekar from the Sanford Research Histology and Imaging Core. We would also like to thank Dr. Xuejun Wang from the University of South Dakota for critical feedback during revision and preparation of this manuscript.

Conflict of Interest

There are no conflicts of interest to disclose.

References

1. Daigle N, Beaudouin J, Hartnell L, Imreh G, Hallberg E, et al. (2001) Nuclear pore complexes form immobile networks and have a very low turnover in live mammalian cells. The Journal of cell biology 154(1): 71-84.
2. Toyama BH, Arrojo EDR, Lev Ram V, Ramachandra R, Deerinck TJ, et al. (2019) Visualization of long-lived proteins reveals age mosaicism within nuclei of postmitotic cells. The Journal of cell biology 218(2): 433-444.
3. Toyama BH, Savas JN, Park SK, Harris MS, Ingolia NT, et al. (2013) Identification of long-lived proteins reveals exceptional stability of essential cellular structures. Cell 154(5): 971-982.
4. Rabut G, Doye V, Ellenberg J (2004) Mapping the dynamic organization of the nuclear pore complex inside single living cells. Nature cell biology 6(11): 1114-1121.
5. Capitanchik C, Dixon CR, Swanson SK, Florens L, Kerr ARW, et al. (2018) Analysis of RNA-Seq datasets reveals enrichment of tissue-specific splice variants for nuclear envelope proteins. Nucleus 9(1): 410-430.
6. Sakuma S, D Angelo MA (2017) the roles of the nuclear pore complex in cellular dysfunction, aging and disease. Semin Cell Dev Biol 68: 72-84.
7. Haskell GT, Jensen BC, Samsa LA, Marchuk D, Huang W, et al. (2017) Whole Exome Sequencing Identifies Truncating Variants in Nuclear Envelope Genes in Patients With Cardiovascular Disease. Circ Cardiovasc Genet 10(3).
8. Burdine RD, Preston CC, Leonard RJ, Bradley TA, Faustino RS (2020) Nucleoporins in cardiovascular disease. J Mol Cell Cardiol 141: 43-52.
9. Zhang X, Chen S, Yoo S, Chakrabarti S, Zhang T, et al. (2008) Mutation in nuclear pore component NUP155 leads to atrial fibrillation and early sudden cardiac death. Cell 135(6): 1017-1027.
10. Zhang L, Tester DJ, Lang D, Chen Y, Zheng J, et al. (2016) Does Sudden Unexplained Nocturnal Death Syndrome Remain the Autopsy-Negative Disorder: A Gross, Microscopic, and Molecular Autopsy Investigation in Southern China. Mayo Clin Proc 91(11): 1503-1514.

11. Kehat I, Accornero F, Aronow BJ, Molkentin JD (2011) Modulation of chromatin position and gene expression by HDAC4 interaction with nucleoporins. The Journal of cell biology 193(1): 21-29.

12. Preston CC, Storm EC, Burdine RD, Bradley TA, Uttecht AD, et al. (2019) Nucleoporin insufficiency disrupts a pluripotent regulatory circuit in a pro-arrhythmogenic stem cell line. Sci Rep 9(1): 12691.

13. Preston CC, Wyles SP, Reyes S, Storm EC, Eckloff BW, et al. (2018) NUP155 insufficiency recalibrates a pluripotent transcriptome with network remodeling of a cardiogenic signaling module. BMC Syst Biol 12(1): 62.

14. Kosova B, Panté N, Rollenhagen C, Podtelejnikov A, Mann M, et al. (2000) Mlp2p, a component of nuclear pore attached intranuclear filaments, associates with nic96p. J Biol Chem 275(1): 343-350.

15. Niepel M, Molloy KR, Williams R, Farr JC, Meinema AC, et al. (2013) The nuclear basket proteins Mlp1p and Mlp2p are part of a dynamic interactome including Esc1p and the proteasome. Mol Biol Cell 24(24): 3920-3938.

16. Albert S, Schaffer M, Beck F, Mosalaganti S, Asano S, et al. (2017) Proteasomes tether to two distinct sites at the nuclear pore complex. Proc Natl Acad Sci USA 114(52): 13726-13731.

17. Gallardo P, Salas Pino S, Daga RR (2017) A new role for the nuclear basket network. Microb Cell 4(12): 423-425.

18. Lupu F, Alves A, Anderson K, Doye V, Lacy E (2008) Nuclear Pore Composition Regulates Neural Stem/Progenitor Cell Differentiation in the Mouse Embryo. Developmental cell (6): 831-842.

19. Mossaid I, Chatel G, Martinelli V, Vaz M, Fahrenkrog B(2020) Mitotic checkpoint protein Mad1 is required for early Nup153 recruitment to chromatin and nuclear envelope integrity. Journal of cell science 133(21).

20. Nanni S, Re A, Ripoli C, Gowran A, Nigro P, et al. (2016) The nuclear pore protein Nup153 associates with chromatin and regulates cardiac gene expression in dystrophic mdx hearts. Cardiovasc Res 112(2): 555-567.

21. Toda T, Hsu JY, Linker SB, Hu L, Schafer ST, et al. (2017) Nup153 Interacts with Sox2 to Enable Bimodal Gene Regulation and Maintenance of Neural Progenitor Cells. Cell Stem Cell 21(5): 618-34 e7.

22. Ishikawa Ankerhold HC, Ankerhold R, Drummen GP (2012) Advanced fluorescence microscopy techniques--FRAP, FLIP, FLAP, FRET and FLIM. Molecules (Basel, Switzerland) 17(4): 4047-4132.

23. Kosinski J, Mosalaganti S, von Appen A, Teimer R, DiGuilio AL, et al. (2016) Molecular architecture of the inner ring scaffold of the human nuclear pore complex. Science 352(6283): 363-365.

24. Savas JN, Toyama BH, Xu T, Yates JR 3rd, Hetzer MW (2012) Extremely long-lived nuclear pore proteins in the rat brain. Science 335(6071): 942.

25. Schwartz M, Travesa A, Martell SW, Forbes DJ (2015) Analysis of the initiation of nuclear pore assembly by ectopically targeting nucleoporins to chromatin. Nucleus 6(1): 40-54.

26. De Magistris P, Tatarek Nossol M, Dewor M, Antonin W (2018) A self-inhibitory interaction within Nup155 and membrane binding are required for nuclear pore complex formation. Journal of cell science 131(1).

27. Busayavalasa K, Chen X, Farrants AK, Wagner N, Sabri N (2012) The Nup155-mediated organisation of inner nuclear membrane proteins is independent of Nup155 anchoring to the metazoan nuclear pore complex. Journal of cell science 125(Pt 18): 4214-4218.

28. Leonard RJ, Preston CC, Gucwa ME, Afeworki Y, Selya AS, et al. (2020) Protein Subdomain Enrichment of NUP155 Variants Identify a Novel Predicted Pathogenic Hotspot. Front Cardiovasc Med 7: 8.

29. Lin DH, Correia AR, Cai SW, Huber FM, Jette CA, et al. (2018) Structural and functional analysis of mRNA export regulation by the nuclear pore complex. Nat Commun 9(1): 2319.

30. Griffis ER, Craige B, Dimaano C, Ullman KS, Powers MA (2004) distinct functional domains within nucleoporins Nup153 and Nup98 mediate transcription-dependent mobility. Mol Biol Cell 15(4): 1991-2002.

31. Kelley K, Knockenhauer KE, Kabachinski G, Schwartz TU (2015) Atomic structure of the Y complex of the nuclear pore. Nat Struct Mol Biol 22(5): 425-431.

32. Eisenhardt N, Redolfi J, Antonin W (2014) Interaction of Nup53 with Ndc1 and Nup155 is required for nuclear pore complex assembly. Journal of cell science 127(Pt 4): 908-921.

33. Vollmer B, Schooley A, Sachdev R, Eisenhardt N, Schneider AM, et al. (2012) Dimerization and direct membrane interaction of Nup53 contribute to nuclear pore complex assembly. EMBO J 31(20): 4072-4084.

34. Fischer J, Teimer R, Amlacher S, Kunze R, Hurt E (2015) Linker Nups connect the nuclear pore complex inner ring with the outer ring and transport channel. Nat Struct Mol Biol 22(10): 774-81.

35. Handa N, Kukimoto Niino M, Akasaka R, Kishishita S, Murayama K, et al. (2006) the crystal structure of mouse Nup35 reveals atypical RNP motifs and novel homodimerization of the RRM domain. J Mol Biol 363(1): 114-124.

36. Xu L, Pan L, Li J, Huang B, Feng J, et al. (2015) Nucleoporin 35 regulates cardiomyocyte pH homeostasis by controlling Na+-H+ exchanger-1 expression. J Mol Cell Biol 7(5): 476-485.

37. Lapetina DL, Ptak C, Roesner UK, Wozniak RW (2017) Yeast silencing factor Sir4 and a subset of nucleoporins form a complex distinct from nuclear pore complexes. The Journal of cell biology 216(10): 3145-3159.

38. Raices M, D Angelo MA (2012) nuclear pore complex composition: a new regulator of tissue-specific and developmental functions. Nat Rev Mol Cell Biol 13(11): 687-699.